

Direct Observational Evidence of Altered Mesosphere Lower Thermosphere Mean Circulation from a Major Sudden Stratospheric Warming

Federico Gasperini¹, McArthur Jones², Brian J Harding³, and Thomas J. Immel³

¹Orion Space Solutions

²United States Naval Research Laboratory

³University of California, Berkeley

December 21, 2022

Abstract

Sudden stratospheric warmings (SSWs) are large-scale phenomena characterized by dramatic dynamic disruptions in the stratospheric winter polar regions. Previous studies, especially those employing whole atmosphere models, indicate that SSWs have strong impacts on the circulation of the mesosphere lower thermosphere (MLT) and drive a reversal in the mean meridional circulation (MMC) near 90-125 km altitude. However, the robustness of these effects and the roles of SSW-induced changes in global-scale wave activity to drive the reversal have been difficult to observe simultaneously. This work employs horizontal lower thermospheric (~93-106 km altitude) winds near 10S-40N latitude from the Michelson Interferometer for Global High-resolution Thermospheric Imaging (MIGHTI) instrument onboard the Ionospheric Connection Explorer (ICON) to present observational evidence of a prominent MLT MMC reversal associated with the January 2021 major SSW event and to demonstrate connections to semidiurnal tidal activity and possible associations with a ~3-day ultra-fast Kevin wave (UFKW).

1 **Direct Observational Evidence of Altered Mesosphere**
2 **Lower Thermosphere Mean Circulation from a Major**
3 **Sudden Stratospheric Warming**

4 **Federico Gasperini¹, McArthur Jones Jr², Brian J. Harding³, Thomas J.**
5 **Immel³**

6 ¹Orion Space Solutions, 282 Century Pl #1000, Louisville, CO, USA

7 ²Space Science Division, U.S. Naval Research Laboratory, Washington, DC, USA

8 ³Space Sciences Laboratory, University of California, Berkeley, CA, USA

9 **Key Points:**

- 10 • A prominent (~ 30 m/s) reversal in the MLT mean meridional circulation during
11 the January 2021 major SSW is observed in MIGHTI winds
- 12 • Strong (~ 35 m/s) MLT westward flow enhancements are observed following the
13 onset of the SSW
- 14 • Amplification in MLT SW2 zonal wind amplitudes are consistent with the observed
15 westward flow enhancements

Abstract

Sudden stratospheric warmings (SSWs) are large-scale phenomena characterized by dramatic dynamic disruptions in the stratospheric winter polar regions. Previous studies, especially those employing whole atmosphere models, indicate that SSWs have strong impacts on the circulation of the mesosphere lower thermosphere (MLT) and drive a reversal in the mean meridional circulation (MMC) near 90-125 km altitude. However, the robustness of these effects and the roles of SSW-induced changes in global-scale wave activity to drive the reversal have been difficult to observe simultaneously. This work employs horizontal lower thermospheric (~ 93 -106 km altitude) winds near 10°S - 40°N latitude from the Michelson Interferometer for Global High-resolution Thermospheric Imaging (MIGHTI) instrument onboard the Ionospheric Connection Explorer (ICON) to present observational evidence of a prominent MLT MMC reversal associated with the January 2021 major SSW event and to demonstrate connections to semidiurnal tidal activity and possible associations with a ~ 3 -day ultra-fast Kevin wave (UFKW).

Plain Language Summary

The winds in the mesosphere lower thermosphere (MLT) are strongly impacted by dramatic changes in the stratospheric winter polar regions associated with Sudden Stratospheric Warmings (SSWs). Models have shown that the climatological direction of the MLT north-south and vertical circulation, characterized by equatorward flow near ~ 100 -120 km and poleward flow near ~ 80 -100 km, reverses following the onset of SSWs. Yet, the impacts and causes of these dynamical effects are not well established observationally due to the lack of comprehensive global measurements of the MLT region. This study evaluates the evolution of MLT winds and associated tidal and ultra-fast Kevin wave (UFKW) variations during the January 2021 SSW using horizontal wind observations from the Michelson Interferometer for Global High-resolution Thermospheric Imaging (MIGHTI) instrument onboard the Ionospheric Connection Explorer (ICON) to present observational evidence of a large MLT north-south wind reversal due to the SSW and associated global-scale wave influences.

1 Introduction

Stratospheric Sudden Warmings (SSWs) are global-scale meteorological events driven by the dissipation of vertically-propagating planetary waves originating in the troposphere

(Matsuno, 1971; Butler et al., 2015). SSW events are characterized based on the changes that occur in the stratosphere, including a rapid increase in polar temperatures and deceleration of the zonal mean zonal winds. A SSW is classified as a major SSW if the zonal mean zonal winds at 60°N and 10 hPa reverse from eastward to westward (e.g., Charlton and Polvani, 2007). SSWs lead to significant disturbances in the whole atmosphere (Stening 1977), producing remarkable changes in composition, dynamics, and electro-dynamics of the whole ionosphere-thermosphere system, pole-to-pole, as demonstrated by a number of modeling and observational studies (e.g., Goncharenko and Zhang 2008; Chau et al. 2009; Goncharenko et al. 2010; Chau et al., 2012, 2015; Butler et al., 2015; Zulicke et al., 2018; Laskar et al., 2019; Pedatella et al., 2014, 2016, 2018, 2022; Jones et al., 2020; Oberheide et al., 2020; Oberheide 2022; Siddiqui et al., 2022; Liu et al., 2022). Modeling and observational evidence also suggest that SSW impacts can extend into the summer mesosphere and mesopause region through inter-hemispheric coupling (e.g., Becker and Fritts, 2006; Tan et al., 2012; Liu et al., 2013, 2014; Miyoshi et al. 2015; Lieberman et al., 2021; Goncharenko et al., 2022). Thus, SSWs provide an exemplary case to study the coupling between the lower atmosphere and the overlying atmospheric regions.

It is now well established that the deceleration and reversal of winter stratospheric wind associated with SSWs produce significant changes in the propagation conditions of global-scale waves that lead to strong changes in upper atmospheric circulation (e.g., Liu and Roble, 2002; Tan et al., 2012; Yiğit and Medvedev, 2012, 2016; Yuan et al., 2012; Yiğit et al., 2014, 2016; Miyoshi et al., 2015; Liu, 2017; Jones et al., 2020). These SSW-induced wind and temperature disturbances in the stratosphere and mesosphere lead to enhancements in the solar semidiurnal migrating tide (SW2, 12-hour period and westward zonal wave number $s = 2$) and other non-migrating tidal components (e.g, Chang et al., 2009; Liu et al., 2010; Pancheva et al., 2009; Pedatella et al., 2012; Pedatella and Liu, 2013) due to nonlinear interactions with stationary planetary waves (e.g., Liu et al. 2010; Sathishkumar and Sridharan, 2013), changes in the tidal propagation conditions (e.g., Jin et al. 2012) and stratospheric ozone distribution (e.g., Goncharenko et al. 2012; Siddiqui et al. 2019). SSWs can also lead to resonant amplification of the lunar semidiurnal migrating tide (M2, 12.42-hour period) because of the atmospheric Pekeris mode (Forbes and Zhang, 2012; Liu et al., 2022). Modeling evidence (e.g., Yamazaki et al., 2020) also suggests that ultra-fast Kelvin waves (UFWs) may be amplified during SSWs, how-

79 ever, the relationship between SSWs and UFKWs remains unclear (e.g., England et al.,
80 2012; Liu et al., 2012; Phanikumar et al., 2014; Sassi et al., 2013, Yamazaki et al., 2020).

81 Previous modeling studies (e.g., Miyoshi et al., 2015; Zhang J. et al., 2021, 2022;
82 Orsolini et al., 2022; Wang et al., 2022) suggest that the climatological direction of the
83 mesosphere-lower thermosphere (MLT) mean meridional circulation (MMC), character-
84 ized by upwelling in the middle winter latitudes, equatorward flow near ~ 100 - 120 km,
85 and poleward flow near ~ 80 - 100 km, reverses following the onset of SSWs. Ground-to-
86 topside model of Atmosphere and Ionosphere for Aeronomy (GAIA) model simulations
87 from Miyoshi et al. (2015) revealed that MMC reversed in the lower thermosphere. More
88 recently, Orsolini et al. (2022) used the Whole Atmosphere Community Climate Model
89 with thermosphere and ionosphere eXtension (WACCM-X) in the specified dynamics con-
90 figuration to show that the lower thermospheric mean meridional circulation reverses for
91 about 10 days following the onset of elevated stratopause events in the northern hemi-
92 sphere largely driven by westward-propagating planetary waves. Important impacts on
93 MLT mean circulation have also been reported observationally (e.g., Oberheide, 2022)
94 including enhancements of both eastward and westward directed flow associated with
95 wave dissipation. Zhang R. et al. (2022) used Ionospheric Connection Explorer (ICON)
96 Michelson Interferometer for Global High-resolution Thermospheric Imaging (MIGHTI)
97 and Ion Velocity Meter (IVM) data to investigate ionosphere-thermosphere coupling dur-
98 ing the January 2021 SSW, suggesting the importance of the F-region northward wind
99 changes in driving anomalous ionospheric field-aligned flows. However, no studies have
100 investigated the lower-altitude wind patterns which are thought to dominate the iono-
101 spheric SSW response.

102 This study examines zonal and meridional MLT (~ 93 - 106 km) wind observations
103 from the MIGHTI instrument onboard ICON to present observational evidence of a promi-
104 nent MLT MMC reversal associated with the January 2021 major SSW event and to demon-
105 strate connections to semidiurnal tidal activity and possible impacts on a ~ 3 -day UFKW
106 with $s = -1$ (hereafter, UFKW1). After a brief description of the data and methods (Sec-
107 tion 2), we show impacts on MLT dynamics and connections to wave drivers (Section
108 3), and provide the conclusions (Section 4).

2 ICON MIGHTI Neutral Wind Profiles and Wave Diagnostics

ICON is a NASA Heliophysics System Observatory (HSO) mission launched on 10 October 2019 into a nearly circular ~ 590 km altitude and $\sim 27^\circ$ inclination orbit to study the connections between the dynamics of the neutral atmosphere near 90-300 km and the electrodynamics of the low-latitude ionosphere (Immel et al., 2018; Immel and Eastes, 2019; Immel et al., 2021). ICON retrieves neutral wind profiles in the upper atmosphere using the Michelson Interferometer for Global High-resolution Thermospheric Imaging (MIGHTI) instrument from remote observations of green ~ 557.7 nm and red ~ 630.0 nm airglow emissions (Harlander et al. 2017). This work employs zonal and meridional neutral winds (ICON data product L2.2 V04) from ~ 93 km to ~ 106 km altitude, where continuous day and night observations are available in the 10°S to 40°N latitude range. More information on MIGHTI wind, error analyses, and validation can be found in Englert et al. (2017), Harding et al. (2017, 2021), and Makela et al. (2021). Recently, Yiğit et al (2022) examined the climatology of MIGHTI mean zonal and meridional winds and associated mean circulation finding the prevalence of eastward zonal winds and northward meridional winds and general agreement with middle thermospheric wind climatologies, validating the use of MIGHTI to study mean winds.

Based on the occurrence of occasional gaps, data quality issues, and instrument calibrations, MIGHTI allows for stable extraction of solar tides within 41-day moving windows (Cullens et al., 2020; Forbes et al., 2022). In this work, semidiurnal tidal fits are performed using 41-day moving windows on winds averaged in 6° latitude, 60° longitude, and 2-hour UT bins extending from 10°S to 40°N using the native ~ 2.5 km altitude sampling. This binning effectively removes the effects of small-scale variations and improves the statistics while also leading to smoother visual depictions. Wind data flagged as bad (quality flag = 0) are not included. Many of the 0-flagged data are connected with South Atlantic Anomaly contamination. Their removal leaves gaps near 270° - 330° longitude in the Southern Hemisphere that are not significantly affecting the latitude regions of primary interest for this study. Forbes et al. (2022) provide more details on the tidal diagnostics of the composite data, which closely follows the procedure adopted by Gasperini et al. (2021) in the analyses of ICON IVM data and by Gasperini et al. (2015, 2017, 2018, 2020) in the analysis of Thermosphere, Ionosphere, Mesosphere, Energetics and Dynamics (TIMED) observations. After the exact UFKW1 period is determined using spectral analysis, simultaneous least-squares fits are performed on these 41-day windows to de-

Figure 1. (a) MERRA-2 zonal and diurnal average zonal wind near 60°N latitude during 1 December 2020 - 31 January 2021. (b) Same as (a), but for MERRA-2 temperature averaged 60°N - 90°N latitude. (c) Time series of (a) at 10 hPa. (d) Time series of F10.7 (black line) and Kp (blue line, left y-axis) for the same period as (a)-(c). The orange vertical lines indicate 3 January 2021 when the zonal mean zonal winds at 60°N and 10 hPa first reversed from eastward to westward.

142 rive SW2 and UFKW1 amplitudes and phases. UFKW1 amplitudes are extracted us-
 143 ing 41-day moving windows for consistency with the tidal diagnostics. Daily ZM winds
 144 are obtained from ICON MIGHTI as the average from the measurements at the ascend-
 145 ing and descending nodes. As noted by Gasperini et al. (2020) who applied a similar method
 146 to Gravity Field and Steady-State Ocean Circulation Explorer (GOCE) data, the ascend-
 147 ing and descending ZM mean winds include both the true ZM and a contribution from
 148 SW2, which is sampled at the same phase on both orbit nodes. Along with aliasing from
 149 SW2, these ZM estimates may also be affected by LT precession, especially near the ter-
 150 minators.

151 **3 Results**

152 Figure 1 shows the height-time structure of the longitude and diurnal mean zonal
 153 wind at 60°N (panel a) and 60° - 90°N polar cap temperature (panel b), the time series
 154 of the zonal mean zonal wind at 10 hPa (panel c) and the time series of the solar and
 155 geomagnetic indices (panel d) for 1 December 2020 - 31 January 2021. A major SSW
 156 event, indicated by a reversal of the 60°N stratospheric zonal mean zonal winds, started
 157 on 3 January 2021, with westward winds that persisted through 21 January (with a 2-
 158 day eastward interruption). The relatively long persistence of westward wind during this
 159 SSW was explained as a reflection of persistent strong dynamical forcing overtaking non-
 160 adiabatic cooling effects (e.g., Lu et al., 2021). More information on the lower and mid-
 161 dle atmospheric response to this SSW can be found in the recent work by Rao et al. (2021).
 162 The geomagnetic Kp index (blue line in Figure 1d) exhibits periods of moderate activ-

Figure 2. MIGHTI longitude-mean day/night averaged meridional winds near 106 km (a) and 93 km (b) during 1 December 2020 - 31 January 2021. (a')-(b') Same as (a)-(b), but for zonal winds. MIGHTI meridional mean winds as a function of altitude (~ 94 -106 km) and latitude (~ 0 -40°N) during 7 December - 2 January (c) and 3-29 January (c'). (c'') Difference between (c') and (c). (d)-(d'') Same as (c)-(c''), but for zonal winds. The orange vertical lines in (a)-(a') and (b)-(b') indicate 3 January 2021 when the zonal mean zonal winds at 60°N and 10 hPa first reversed from eastward to westward.

163 ity, with values exceeding 4 on six occasions during 1 December - 31 January. The F10.7
 164 solar flux index (black line in Figure 1d) decreases from a maximum near 110 sfu on De-
 165 cember 1 to near 80 sfu on December 7, remaining relatively constant through January
 166 31. It is important to note that the recurrent moderate geomagnetic activity present dur-
 167 ing this 62-day period is unlikely to generate variability at MLT heights that would sig-
 168 nificantly alias into the dynamic response to the SSW, especially considering that its day-
 169 to-day variability is very different than the timescale of the SSW (see the discussion in
 170 Oberheide (2022)).

171 Next, the dynamic response of the MLT to the SSW is examined by employing longitude-
 172 and day/night-averaged (hereafter, 'zonal mean') MIGHTI wind observations between
 173 ~ 93 km and ~ 106 km. Figure 2 shows the temporal evolution of zonal mean MIGHTI
 174 meridional (panels *a* and *b*) and zonal (panels *a'* and *b'*) winds as a function of latitude
 175 (10°S - 35°N) during 1 December 2020 - 31 January 2021 near 106 km and 93 km, respec-
 176 tively. After removing seasonal and longer-term effects by generating residuals from 27-
 177 day running means, the winds are then averaged between Dec 7 - Jan 2 ('Before SSW')
 178 and Jan 3 - Jan 29 ('During SSW'), and their altitude (~ 94 -106 km) and latitude (~ 0 -
 179 40°N) structure is illustrated in Figures 2*c*-2*c'* (Figures 2*d*-2*d'*) for the meridional (zonal)
 180 components. To best highlight changes associated with the SSW, Figure 2*c''* (Figure 2*d''*)
 181 shows the differences between the 'During SSW' and the 'Before SSW' case for the merid-
 182 ional (zonal) wind component. As visible by close inspection of Figures 2*a*-2*b* and best

Figure 3. ICON/MIGHTI mean zonal winds near 93 km (a), MIGHTI 41-day mean zonal wind SW2 (b), SW1 (c), SW3 (d), and UFKW1 (e) amplitudes near 93 km during 1 Dec 2020 - 31 Jan 2021. (a')-(e') Same as (a)-(d), but near 106 km. The orange vertical lines indicate 3 January 2021 when the zonal mean zonal winds at 60°N and 10 hPa first reversed from eastward to westward.

183 illustrated by Figure 2c'', the meridional mean winds are found to experience a marked
 184 change in direction from primarily southward before the SSW to primarily northward
 185 during the SSW at the upper heights (i.e., above ~98 km) and from mainly northward
 186 before the SSW to mainly southward during the SSW at the lower MLT heights (i.e.,
 187 ~95-98 km). These effects are particularly prominent near 20°N-40°N with meridional
 188 wind variations around 10-40 m/s (depending on latitude and altitude). The direction
 189 and magnitude of these wind variations provide observational confirmation of previous
 190 modeling results (e.g., Miyoshi et al., 2015) and are consistent with the understanding
 191 that the typical summer-to-winter MLT flow can be broken down during SSWs, result-
 192 ing in a two-cell pattern with equatorward motion at lower heights (i.e., <90-95 km) and
 193 poleward motion aloft (i.e., >105-110 km).

194 Prominent enhancements in the westward mean winds following the onset of the
 195 SSW are found, with variations up to ~35 m/s compared to the 'Before SSW' case as
 196 demonstrated by Figure 2d''. These effects exhibit a strong dependency in latitude and
 197 some in altitude, with the westward enhancements strongest at the northernmost lat-
 198 itudes sampled by MIGHTI (i.e., ~30°N-40°N). Further, previous modeling work by Miyoshi
 199 et al. (2015), Oberheide et al. (2020), and Jones et al. (2020) indicate that these enhanced
 200 westward winds observed by MIGHTI are likely driven by periodic westward forcing via
 201 the Eliassen-Palm flux divergence, which then contributes to the observed residual MMC
 202 in Figure 2.

203 Finally, the response of MLT zonal wind wave amplitudes to the SSW is examined
 204 using 41-day running averages of MIGHTI observations. While a 35-day averaging may

205 be sufficient to extract the complete tidal spectrum from MIGHTI data (e.g., Cullens
206 et al., 2020), we find that a 41-day averaging provides improved fits for latitudes above
207 $\sim 25^\circ\text{N}$ (see also discussion in Section 2). Figure 3 shows MIGHTI mean zonal winds near
208 93 km (panel *a*) and 106 km (panel *a'*) and SW2, SW1, and SW3 zonal wind tidal am-
209 plitudes near 93 km (panels *b-d*) and near 106 km (panels *b'-d'*). Large enhancements
210 in SW2 zonal wind amplitudes near 93 km and 10°N - 35°N occur around 10-20 January
211 concurrent with the significant strengthening in westward mean winds that follows the
212 onset of the SSW. A weaker increase in SW2 amplitudes (and enhanced westward mean
213 winds) also appears near the equator during 1-7 January. Similar to the SW2 MIGHTI
214 wind diagnostics in Oberheide (2022), SW2 displays strong enhancements associated with
215 the SSW near 106 km. SW1, SW2, and SW3 typically attain their largest amplitudes
216 at mid-to-high latitudes, outside of the latitudes observed by ICON. However, recent work
217 by Pedatella (2022) shows that simulated SD-WACCM-X SW2 amplitudes near 110 km
218 are also strongly enhanced between 1-8 January near 50°N - 60°N and 50°S - 60°S , with
219 SD-WACCM-X SW1 and SW3 zonal wind amplitudes also slightly enhanced but exhibit-
220 ing more day-to-day variability. Also, note that while SSW-induced effects on SW1 and
221 SW3 seem less prominent than those observed on SW2, it is important to keep in mind
222 that day-to-day variability in these tidal components is largely removed by the 41-day
223 averaging.

224 In addition to the semidiurnal tidal impacts previously noted, evidence of a large
225 (~ 15 m/s near 106 km) ~ 3 -day UFKW1 is found during this 62-day period extending
226 from 1 December 2020 to 31 January 2021. Figures 2e-2e' show the latitude-temporal
227 structure of its amplitudes during 1 December - 31 January near 93 km and 106 km, re-
228 spectively. Enhanced UFKW1 amplitudes near 106 km observed during 11-21 January
229 and ~ 0 - 10°N closely resemble the SW2 amplifications found near 93 km. Connections
230 between SSWs and UFKWs are not unexpected, as enhanced westward mean winds in
231 the middle atmosphere would tend to favor the vertical propagation of UFKWs into the
232 MLT given their eastward-propagation characteristics. It is well known both numerically
233 and observationally (e.g., Forbes, 2000, 2020; Gasperini et al., 2015, 2018, 2020) that back-
234 ground zonal-mean zonal winds can Doppler-shift UFKWs modifying their propagation
235 (e.g., Ekanayake et al., 1997), and thus changing their vertical wavelength (e.g., Forbes
236 and Vincent, 1989) and susceptibility to dissipation. While of certain interest, it would

237 be beyond the scope of this study to investigate SSW-UFKW connections in further de-
238 tail and this effort is left as an avenue for possible follow on work.

239 **4 Summary and Conclusions**

240 Previous whole atmosphere modeling studies suggest that the climatological direc-
241 tion of the MLT mean meridional circulation, characterized by equatorward flow near
242 ~ 100 - 120 km and poleward flow near ~ 80 - 100 km, reverses in response to a major SSW
243 event. However, the veracity of these modeling predictions, the robustness of the effects,
244 and the roles of SSW-induced changes in global-scale activity to drive the reversal have
245 yet to be observed concurrently.

246 This work employed zonal and meridional MLT wind observations from the MIGHTI
247 instrument onboard ICON in the ~ 93 - 106 km altitude range to present first-time (to the
248 best of the authors' knowledge) observational evidence of a prominent MLT MMC re-
249 versal associated with the January 2021 major SSW event. The meridional mean winds
250 are found to change in direction from southward before the SSW to northward during
251 the SSW at the upper heights (i.e., above ~ 98 km) and from northward before the SSW
252 to southward during the SSW at the lower MLT heights (i.e., ~ 95 - 98 km). These large
253 changes in the mean meridional winds are of the order of ± 30 m/s and are most promi-
254 nent at the northernmost latitudes sampled by MIGHTI (i.e., 30 - 40°N). These wind changes
255 provide observational confirmation of previous modeling results (e.g., Miyoshi et al., 2015)
256 suggesting that the typical summer-to-winter MLT flow is broken down during SSWs and
257 a resulting two-cell pattern emerges with equatorward motion at lower heights and pole-
258 ward motion aloft.

259 Prominent enhancements (upward of ~ 35 m/s) in westward mean winds are also
260 found in response to the SSW, with effects that are strongest at higher altitudes (i.e.,
261 > 102 km) and latitudes (i.e., $\sim 30^\circ$ - 40°N). Large enhancements in SW2 zonal wind am-
262 plitudes near 93 km and 10°N - 35°N occurring around 10-20 January are concurrent and
263 nearly colocated with significant strengthening in westward mean winds following the
264 onset of the SSW. Effects associated with SW1 and SW3 are found to play a smaller role,
265 in contrast with the discussion by Zhang R. et al (2022). Spectral analyses also reveal
266 the presence of a ~ 3 -day UFKW1 with enhanced amplitudes (~ 15 m/s) near 106 km
267 occurring during 10-20 January and 0 - 10°N that closely resemble the SW2 amplifications

268 near 93 km. The latter result supports a possible connection between SSWs and UFKWs
 269 that warrants further investigation.

270 5 Open Research

271 MIGHTI ICON V04 winds were obtained from [https://icon.ssl.berkeley.edu/
 272 Data/](https://icon.ssl.berkeley.edu/Data/). Note that preliminary analyses of the recently-released MIGHTI V05 wind prod-
 273 uct support the main conclusions of this study. The 3-hourly Kp index was obtained from
 274 GFZ Potsdam at https://kp.gfz-potsdam.de/app/files/Kp_ap_since_1932.txt, the
 275 F10.7 cm radio flux from NASA/GSFC OMNIWeb at [https://omniweb.gsfc.nasa.gov/
 276 form/dx1.html](https://omniweb.gsfc.nasa.gov/form/dx1.html), and the MERRA-2 zonal wind and temperature from NASA/GSFC Global
 277 Modeling and Assimilation Office (GMAO) at [https://gmao.gsfc.nasa.gov/reanalysis/
 278 MERRA-2/data_access/](https://gmao.gsfc.nasa.gov/reanalysis/MERRA-2/data_access/).

279 Acknowledgments

280 ICON is supported by NASA's Explorers Program through contracts NNG12FA45C and
 281 NNG12FA42I. FG acknowledges support from NASA Grant No. 80NSSC22K0019 and
 282 NSF Award No. 2113411. MJ acknowledges support from the NASA Early Career In-
 283 vestigator (NNH18ZDA001N-ECIP/18-ECIP_2-0018) and GOLD-ICON Guest Investi-
 284 gators (NNH20ZDA001N-GIGI/20-GIGI20_2-0009) programs.

285 References

- 286 Becker, E., and D. C. Fritts, 2006: Enhanced gravity-wave ac- tivity and interhemi-
 287 spheric coupling during the macwave/ midas northern summer program 2002.
 288 *Ann. Geophys.*, 24, 1175-1188.
- 289 Butler, A. H., Seidel, D. J., Hardiman, S. C., Butchart, N., Birner, T., and Match,
 290 A. (2015). Defining Sudden Stratospheric Warmings. *Bulletin of the American
 291 Meteorological Society*, 96(11), 1913-1928, doi:10.1175/bams-d-13- 00173.1
- 292 Chang, L. C., Palo, S. E., and Liu, H.-L. (2009). Short-term variation of the $s = 1$
 293 nonmigrating semidiurnal tide during the 2002 stratospheric sudden warming.
 294 *Journal of Geophysical Research*, 114, D03109, doi:10.1029/2008JD010886
- 295 Charlton, A.J.; Polvani, L.M. A New Look at Stratospheric Sudden Warmings. Part
 296 I: Climatology and Modeling Benchmarks. *J.Clim.* 2007, 20, 449-469.

- 297 Chau, J.L.; Fejer, B.G.; Goncharenko, L.P. Quiet variability of equatorial $E \times B$
 298 drifts during a sudden stratospheric warming event, *Geophys. Res. Lett.* 2009,
 299 36, L05101.
- 300 Chau, J.-L., Goncharenko, L.-P., Fejer, B.-G., and Liu, H. L. (2012), Equatorial and
 301 low latitude ionospheric effects during sudden stratospheric warming events.
 302 *Space Science Reviews*, 168, 385-417, doi:10.1007/s11214-011-9797-5
- 303 Chau, J.-L., Hoffmann, P., Pedatella, N.-M., Matthias, V., and Stober, G. (2015),
 304 Upper mesospheric lunar tides over middle and high latitudes during sudden
 305 stratospheric warming events, *Journal of Geophysical Research: Space Physics*,
 306 120, 3084-3096, doi:10.1002/2015ja020998
- 307 Cullens, C.Y., Immel, T.J., Triplett, C.C. et al. (2020), Sensitivity study for ICON
 308 tidal analysis, *Prog Earth Planet Sci*, 7, 18, doi:10.1186/s40645-020-00330-6
- 309 Ekanayake, E.M.P., Aso, T., & S. Miyahara (1997), Background wind effect on prop-
 310 agation of nonmigrating diurnal tides in the middle atmosphere, *J. Atmos.*
 311 *Solar-Terr. Phys.*, 59, 401-429.
- 312 England, S. L., Liu, G., Zhou, Q., Immel, T. J., Kumar, K. K., & Ramkumar, G.
 313 (2012), On the signature of the quasi-3-day wave in the thermosphere dur-
 314 ing the January 2010 URSI World Day Campaign, *Journal of Geophysical*
 315 *Research*, 117, A06304, doi:10.1029/2012JA017558
- 316 Englert, C. R., Harlander, J. M., Brown, C. M., Marr, K. D., Miller, I. J., Stump, J.
 317 E., et al. (2017), Michelson interferometer for global high-resolution thermo-
 318 spheric imaging (MIGHTI): Instrument design and calibration, *Space Science*
 319 *Reviews*, 212(1-2), 553-584, doi:10.1007/s11214-017-0358-4
- 320 Forbes, J.M. (2000), Wave coupling between the lower and upper atmosphere: Case
 321 study of an ultra-fast kelvin wave, *J. Atmos. Sol. Terr. Phys.*, 62, 1603-1621.
- 322 Forbes, J.M., Vincent, R.A. (1989), Effects of mean winds and dissipation on the
 323 diurnal propagating tide: an analytic approach, *Planet, Space Sci.* 37, 197-209.
- 324 Forbes, J. M., and Zhang, X. (2012), Lunar tide amplification during the January
 325 2009 stratosphere warming event: Observations and theory, *Journal of Geo-*
 326 *physical Research*, 117(A12), doi:10.1029/2012JA017963
- 327 Forbes, J. M., Maute, A., & Zhang, X. (2020), Dynamics and electrodynamics of
 328 an ultra-fast Kelvin wave (UFWK) packet in the ionosphere-thermosphere
 329 (IT), *Journal of Geophysical Research: Space Physics*, 125, e2020JA027856,

- 330 doi:10.1029/2020JA027856
- 331 Forbes, J. M., Oberheide, J., Zhang, X., Cullens, C., Englert, C. R., Harding, B. J.,
 332 et al. (2022), Vertical coupling by solar semidiurnal tides in the thermosphere
 333 from ICON/MIGHTI measurements, *Journal of Geophysical Research: Space*
 334 *Physics*, 127, doi:10.1029/2022JA030288
- 335 Gasperini F, Forbes JM, Doornbos EN, Bruinsma SL (2015), Wave coupling between
 336 the lower and middle thermosphere as viewed from TIMED and GOCE, *J*
 337 *Geophys Res* 120:5788-05804, doi:10. 1002/2015JA021300
- 338 Gasperini F, Hagan ME, Zhao Y (2017), Evidence of tropospheric 90-day oscillations
 339 in the thermosphere, *Geophys Res Lett.*, doi:10.1002/2017GL075445
- 340 Gasperini F, Forbes JM, Doornbos EN, Bruinsma SL (2018), Kelvin wave coupling
 341 from TIMED and GOCE: inter/intra-annual variability and solar activity
 342 effects, *J Atmos Sol-Terr Phys* 171, 176-187, doi:10.1016/j.jastp.2017.08.034
- 343 Gasperini F, Liu H, McInerney J (2020), Preliminary evidence of Madden-Julian
 344 oscillation effects on ultra- fast tropical waves in the thermosphere. *J Geophys*
 345 *Res* 125, doi:10.1029/ 2019JA027649
- 346 Gasperini F, Azeem I, Crowley G, Perdue M, Depew M, Immel T et al. (2021),
 347 Dynamical coupling between the low-latitude lower thermosphere and
 348 ionosphere via the non-migrating diurnal tide as revealed by concurrent
 349 satellite observations and numerical modeling, *Geophys Res Lett*, 48,
 350 doi:10.1029/2021GL093277
- 351 Goncharenko, L., Zhang, S.R. (2008), Ionospheric signatures of sudden stratospheric
 352 warming: Ion temperature at middle latitude, *Geophys. Res. Lett.*, 35, L21103.
- 353 Goncharenko, L.P., Chau, J.L., Liu, H.L., Coster, A.J. (2010), Unexpected con-
 354 nections between the stratosphere and ionosphere, *Geophys. Res. Lett.*, 37,
 355 L10101.
- 356 Goncharenko LP, Coster AJ, Plumb RA, Domeisen DIV (2012), The potential role
 357 of stratospheric ozone in the stratosphere-ionosphere coupling during strato-
 358 spheric warmings, *Geophys Res Lett* 39, doi:10.1029/2012GL051261
- 359 Goncharenko, L. P., Harvey, V. L., Randall, C. E., Coster, A. J., Zhang,
 360 S.-R., Zalizovski, A., et al. (2022), Observations of Pole-to-Pole,
 361 stratosphere-to-ionosphere connection, *Front. Astron. Space Sci.* 8,
 362 doi:10.3389/fspas.2021.768629

- 363 Harding, B. J., Chau, J. L., He, M., Englert, C. R., Harlander, J. M., Marr, K. D.,
 364 et al. (2021), Validation of ICON-MIGHTI thermospheric wind observations:
 365 2. Green-line comparisons to specular meteor radars. *Journal of Geophysical*
 366 *Research: Space Physics*, 126(3), 1-12, doi:10.1029/2020JA028947
- 367 Harding, B. J., Makela, J. J., Englert, C. R., Marr, K. D., Harlander, J. M., Eng-
 368 land, S. L., and Immel, T. J. (2017), The MIGHTI wind retrieval algorithm:
 369 Description and verification. *Space Science Reviews*, 212(1-2), 585-600,
 370 doi:10.1007/s11214-017-0359-3
- 371 Harlander, J. M., Englert, C. R., Brown, C. M., Marr, K. D., Miller, I. J., Zastera,
 372 V., et al., (2017), Michelson Interferometer for Global High-Resolution Ther-
 373 mospheric Imaging (MIGHTI): Monolithic Interferometer Design and Test,
 374 *Space Science Reviews*, 212(1-2), 601-613, doi:10.1007/s11214-017-0358-4
- 375 Immel, T. J., England, S. L., Mende, S. B., Heelis, R. A., Englert, C. R., Edelstein,
 376 J., et al. (2018), The ionospheric connection explorer mission: Mission goals
 377 and design, *Space Science Reviews*, 214(1), 13, doi:10.1007/s11214-017-0449-2
- 378 Immel TJ, Eastes RW (2019), New NASA missions focus on terrestrial forcing of the
 379 space environment, *Bull Am Meteorol Soc* 100:2153-2156, doi:10.1175/BAMS-
 380 D-19-0066.1
- 381 Immel TJ, Harding BJ, Heelis RA, Maute A, Forbes JM, England SL et al. (2021),
 382 Regulation of ionospheric plasma velocities by thermospheric winds, *Nat*
 383 *Geosci* 14:893-898, doi:10.1038/s41561-021-00848-4
- 384 Jin, H., Miyoshi, Y., Pancheva, D., Mukhtarov, P., Fujiwara, H., and Shinagawa,
 385 H. (2012), Response of migrating tides to the stratospheric sudden warming
 386 in 2009 and their effects on the ionosphere studied by a whole atmosphere-
 387 ionosphere model GAIA with COSMIC and TIMED/ SABER observations,
 388 *Journal of Geophysical Research*, 117, A10323, doi:10.1029/2012JA017650
- 389 Jones, M. Jr., Siskind, D. E., Drob, D. P., McCormack, J. P., Emmert, J. T.,
 390 Dhadly, M. S., et al. (2020), Coupling from the middle atmosphere to the
 391 exobase: Dynamical disturbance effects on light chemical species, *Journal of*
 392 *Geophysical Research: Space Physics*, 125, doi:10.1029/2020JA028331
- 393 Laskar, F. I., McCormack, J. P., Chau, J. L., Pallamraju, D., Hoffmann, P., and
 394 Singh, R. P. (2019), Interhemispheric meridional circulation during sudden
 395 stratospheric warming. *Journal of Geophysical Research: Space Physics*, 124,

- 396 7112-7122, doi:10.1029/2018JA026424
- 397 Lieberman, R. S., France, J., Ortland, D. A., and Eckermann, S. D. (2021), The role
398 of inertial instability in cross-hemispheric coupling. *Journal of the Atmospheric*
399 *Sciences*, 78(4), 1113–1127, doi:10.1175/JAS-D-20-0119.1
- 400 Liu, H. L. (2017), Gravity Wave Variation from the Troposphere to the Lower Ther-
401 mosphere during a Stratospheric Sudden Warming Event: A Case Study,
402 SOLA, 13 (Special Edition), 24-30.
- 403 Liu, H.-L., and R. G. Roble (2002), A study of a self-generated stratospheric sud-
404 den warming and its mesospheric/lower thermospheric impacts using coupled
405 TIME-GCM/CCM3, *J. Geophys. Res.*, 107, doi:10.1029/2001JD001533.
- 406 Liu, H.-L., Wang, W., Richmond, A. D., and Roble, R. G. (2010), Ionospheric vari-
407 ability due to planetary waves and tides for solar minimum conditions. *Journal*
408 *of Geophysical Research*, 115, A00G01, doi:10.1029/2009ja015188
- 409 Liu, H., H. Jin, Y. Miyoshi, H. Fujiwara, and H. Shinagawa (2013), Upper atmo-
410 sphere response to stratosphere sudden warming: Local time and height
411 dependence simulated by gaia model. *Geophys. Res. Lett.*, 40, 635-640,
412 doi:10.1002/grl.50146.
- 413 Liu, H., Y. Miyoshi, S. Miyahara, H. Jin, H. Fujiwara, and H. Shinagawa (2014),
414 Thermal and dynamical changes of the zonal mean state of the thermosphere
415 during the 2009 SSW: Gaia simulations. *J. Geophys. Res.: Space Phys.*, 119,
416 6784-6791, doi:10.1002/2014JA020222.
- 417 Liu, J., Zhang, D., Sun, S., Hao, Y., and Xiao, Z. (2022), Ionospheric semi-diurnal
418 lunitidal perturbations during the 2021 Sudden Stratospheric Warming
419 event: Latitudinal and inter-hemispheric variations in the American, Asian-
420 Australian, and African-European sectors. *Journal of Geophysical Research:*
421 *Space Physics*, e2022JA030313.
- 422 Liu, G., England, S. L., Immel, T. J., Kumar, K. K., Ramkumar, G., & Gon-
423 charenko, L. P. (2012), Signatures of the 3-day wave in the low-latitude and
424 midlatitude ionosphere during the January 2010 URSI World Day campaign.
425 *Journal of Geophysical Research*, 117, A06305, doi:10.1029/2012JA017588
- 426 Liu, G., Janches, D., Ma, J., Lieberman, R. S., Stober, G., Moffat-Griffin, T., et al.
427 (2022), Mesosphere and lower thermosphere winds and tidal variations during
428 the 2019 Antarctic Sudden Stratospheric Warming. *Journal of Geophysical*

- 429 Research: Space Physics, 127, e2021JA030177, doi:10.1029/2021JA030177
- 430 Lu, Q., Rao, J., Liang, Z., Guo, D., Luo, J., Liu, S., et al. (2021), The sudden
431 stratospheric warming in January 2021, *Environmental Research Letters*,
432 16(8), 084029.
- 433 Makela, J. J., Baughman, M., Navarro, L. A., Harding, B. J., Englert, C. R., Har-
434 lander, J. M., et al. (2021), Validation of ICON-MIGHTI thermospheric
435 wind observations: 1. Nighttime red-line ground-based Fabry-Perot inter-
436 ferometers, *Journal of Geophysical Research: Space Physics*, 126(2), 1-29,
437 doi:10.1029/2020JA028726.
- 438 Matsuno, T. A Dynamical Model of the Stratospheric Sudden Warming. *J. Atmos.*
439 *Sci.* 1971, 28, 1479-1494.
- 440 Miyoshi, Y., H. Fujiwara, H. Jin, and H. Shinagawa (2015), Impacts of sudden
441 stratospheric warming on general circulation of the thermosphere, *J. Geophys.*
442 *Res. Space Phys.*, 120, 10897-10912, 2015JA021894.
- 443 Oberheide, J., Pedatella, N. M., Gan, Q., Kumari, K., Burns, A. G., and Eastes, R.
444 W. (2020), Thermospheric composition O/N₂ response to an altered merid-
445 ional mean circulation during Sudden Stratospheric Warmings observed by
446 GOLD, *Geophysical Research Letters*, 47(1), doi:10.1029/2019GL086313
- 447 Oberheide, J. (2022), Day-to-day variability of the semidiurnal tide in the F-region
448 ionosphere during the January 2021 SSW from COSMIC-2 and ICON, *Geo-*
449 *physical Research Letters*, 49, doi:10.1029/2022GL100369
- 450 Orsolini, Y. J., Zhang, J., and Limpasuvan, V. (2022), Abrupt Change in the Lower
451 Thermospheric Mean Meridional Circulation during Sudden Stratospheric
452 Warmings and its Impact on Trace Species, *Journal of Geophysical Research:*
453 *Atmospheres*, doi:10.1029/2022JD037050
- 454 Pancheva, D., Mukhtarov, P., and Andonov, B. (2009), Nonmigrating tidal activity
455 related to the sudden stratospheric warming in the Arctic winter of 2003/2004,
456 *Annales Geophysicae*, 27, 975-987, doi:10.5194/angeo-27-975-2009
- 457 Pedatella, N. M., and Liu, H.-L. (2013), The influence of atmospheric tide and
458 planetary wave variability during sudden stratosphere warmings on the
459 low latitude ionosphere. *Journal of Geophysical Research*, 118, 5333-5347,
460 doi:10.1002/jgra.50492

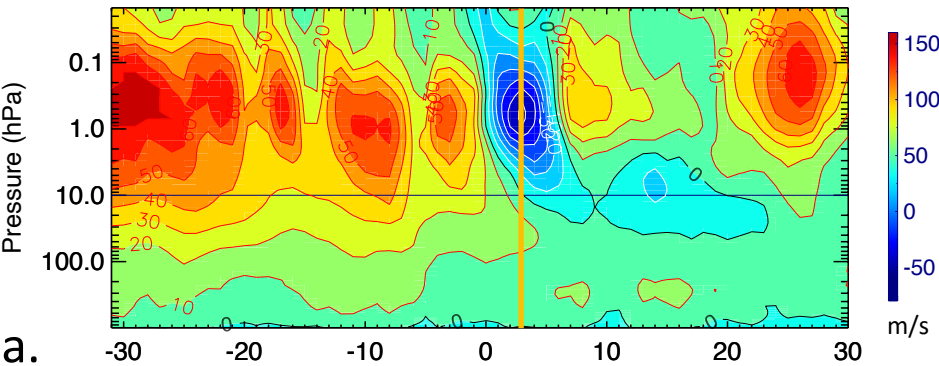
- 461 Pedatella, N. M., Liu, H.-L., Richmond, A. D., Maute, A., and Fang, T.-W. (2012),
 462 Simulations of solar and lunar tidal variability in the mesosphere and lower
 463 thermosphere during sudden stratosphere warmings and their influence on
 464 the low-latitude ionosphere, *Journal of Geophysical Research*, 117, A08326,
 465 doi:10.1029/2012ja017858
- 466 Pedatella, N., Liu, H. L., Sassi, F., Lei, J., Chau, J., and Zhang, X. (2014), Iono-
 467 sphere variability during the 2009 SSW: Influence of the lunar semidiurnal tide
 468 and mechanisms producing electron density variability. *Journal of Geophysical*
 469 *Research: Space Physics*, 119, 3828-3843, doi:10.1002/2014ja019849
- 470 Pedatella, N.-M., Fang, T. W., Jin, H., Sassi, F., Schmidt, H., Chau, J.-L., et al.
 471 (2016), Multimodel comparison of the ionosphere variability during the 2009
 472 sudden stratosphere warming. *Journal of Geophysical Research: Space Physics*,
 473 121, 7204-7225, doi:10.1002/ 2016ja022859
- 474 Pedatella, N.M., Chau, J.L., Schmidt, H., Goncharenko, L.P., Stolle, C., Hocke,
 475 K., Harvey, V.L., Funke, B., Siddiqui, T.A (2018), How sudden stratospheric
 476 warming affects the whole atmosphere, *EOS*, 99, 35-38.
- 477 Pedatella, N. (2022), Ionospheric variability during the 2020-2021 SSW: COSMIC-
 478 2 observations and WACCM-X simulations, *Atmosphere*, 13(3), 368,
 479 doi:10.3390/atmos13030368
- 480 Phanikumar, D., Kumar, K. N., & Kumar, S. (2014), Signatures of ultra-fast Kelvin
 481 waves in low latitude ionospheric TEC during January 2009 stratospheric
 482 warming event, *Journal of Atmospheric and Solar-Terrestrial Physics*, 117,
 483 48-53.
- 484 Rao, J., Garfinkel, C. I., Wu, T., Lu, Y., Lu, Q., and Liang, Z. (2021), The Jan-
 485 uary 2021 sudden stratospheric warming and its prediction in subseasonal
 486 to seasonal models, *Journal of Geophysical Research: Atmospheres*, 126,
 487 doi:10.1029/2021JD035057
- 488 Sassi, F., Liu, H. L., Ma, J., & Garcia, R. R. (2013), The lower thermosphere during
 489 the Northern Hemisphere winter of 2009: A modeling study using high-altitude
 490 data assimilation products in WACCM-X, *Journal of Geophysical Research:*
 491 *Atmospheres*, 118, 8954-8968.
- 492 Sathishkumar, S., and Sridharan, S. (2013), Lunar and solar tidal variabilities in
 493 mesospheric winds and EEJ strength over Tirunelveli (8.7N, 77.8E) during the

- 494 2009 major stratospheric warming, *Journal of Geophysical Research: Space*
495 *Physics*, 118(1), 533-541, doi:10.1029/2012JA018236
- 496 Siddiqui TA, Maute A, Pedatella NM (2019), On the importance of interactive ozone
497 chemistry in Earth-System models for studying mesosphere-lower thermosphere
498 tidal changes during sudden stratospheric warmings, *J Geophys Res Space*
499 *Phys* 124(12), 10690-10707, doi:10.1029/2019JA027193
- 500 Siddiqui, T. A., Chau, J. L., Stolle, C., and Yamazaki, Y. (2022), Migrating solar
501 diurnal tidal variability during Northern and Southern Hemisphere Sudden
502 Stratospheric Warmings, *Earth, Planets and Space*, 74(1), 1-17.
- 503 Stening, R.J. (1977), Electron density profile changes associated with the equatorial
504 electrojet, *J. Atmos. Terr. Phys.*, 39, 157-164.
- 505 Tan, B., X. Chu, H.-L. Liu, C. Yamashita, and J. M. R. III (2012), Zonal-mean
506 global teleconnection from 15 to 110 km derived from saber and waccm, *J.*
507 *Geophys. Res.*, doi:10.1029/ 2011JD016750.
- 508 Wang, J. C., Yue, J., Wang, W., Qian, L., Wu, Q., and Wang, N. (2022), The
509 lower thermospheric winter-to-summer meridional circulation: 1. Driv-
510 ing mechanism, *Journal of Geophysical Research: Space Physics*, 127,
511 doi:10.1029/2022JA030948
- 512 Yamazaki, Y., Miyoshi, Y., Xiong, C., Stolle, C., Soares, G., and Yoshikawa, A.
513 (2020), Whole atmosphere model simulations of ultra-fast Kelvin wave effects
514 in the ionosphere and thermosphere. *Journal of Geophysical Research: Space*
515 *Physics*, 125, doi:10.1029/2020JA027939
- 516 Yiğit, E., and Medvedev, A. S. (2012), Gravity waves in the thermosphere during a
517 sudden stratospheric warming, *Geophysical Research Letters*, 39, L21101.
- 518 Yiğit, E., and Medvedev, A. S. (2016), Role of gravity waves in vertical cou-
519 pling during sudden stratospheric warmings, *Geoscience Letters*, 3, 27,
520 doi:10.1186/s40562-016-0056-1
- 521 Yiğit, E., Medvedev, A. S., England, S. L., and Immel, T. J. (2014), Simulated vari-
522 ability of the high-latitude thermosphere induced by small-scale gravity waves
523 during a sudden stratospheric warming, *Journal of Geophysical Research:*
524 *Space Physics*, 119, 357-365.
- 525 Yiğit, E., P. K. Knížová, K. Georgieva, and W. Ward (2016), A review of vertical
526 coupling in the atmosphere-ionosphere system: Effects of waves, sudden strato-

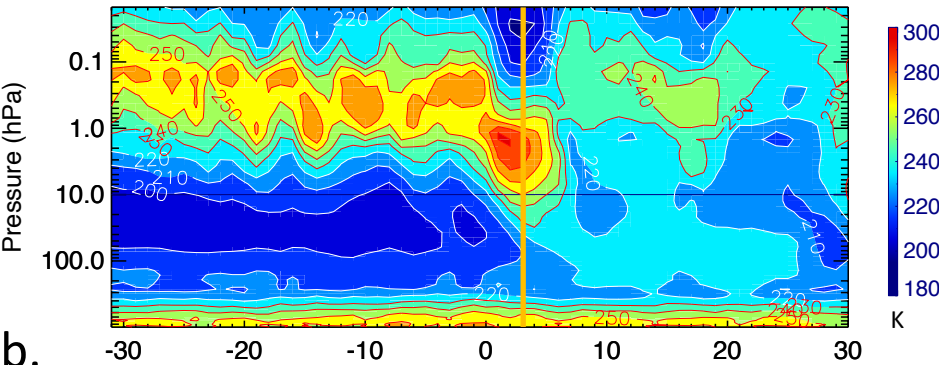
- 527 spheric warmings, space weather, and of solar activity, *J. Atmos. Sol. Terr.*
 528 *Phys.*, 141, 1-12, doi:10.1016/j.jastp.2016.02.011.
- 529 Yiğit, E., Dhadly, M., Medvedev, A. S., Harding, B. J., Englert, C. R., Wu, Q., and
 530 Immel, T. J. (2022), Characterization of the Thermospheric Mean Winds and
 531 Circulation during Solstice using ICON/MIGHTI Observations, *Journal of*
 532 *Geophysical Research: Space Physics*, 127, doi:10.1029/2022JA030851
- 533 Yuan, T., B. Thuraiajah, C.-Y. She, A. Chandran, R. L. Collins, and D. A. Krueger
 534 (2012), Wind and temperature response of midlatitude mesopause region
 535 to the 2009 sudden stratospheric warming, *J. Geophys. Res.*, 117, D09114,
 536 doi:10.1029/2011JD017142
- 537 Zhang, J., Limpasuvan, V., Orsolini, Y. J., Espy, P. J., and Hibbins, R. E. (2021),
 538 Climatological westward-propagating semidiurnal tides and their composite re-
 539 sponse to sudden stratospheric warmings in SuperDARN and SD-WACCM-X,
 540 *J. Geophys. Res. Atm.*, 126, doi:10.1029/2020JD032895
- 541 Zhang, J., Y. Orsolini, V. Limpasuvan (2022), Abrupt Change in the Lower Thermo-
 542 spheric Mean Meridional Circulation during Sudden Stratospheric Warm-
 543 ings and its Impact on Trace Species, CEDAR Workshop MLT Poster,
 544 [https://cedarscience.org/poster-2022/abrupt-change-lower-thermospheric-](https://cedarscience.org/poster-2022/abrupt-change-lower-thermospheric-mean-meridional-circulation-during-sudden)
 545 [mean-meridional-circulation-during-sudden](https://cedarscience.org/poster-2022/abrupt-change-lower-thermospheric-mean-meridional-circulation-during-sudden)
- 546 Zhang, R., Liu, L., Ma, H., Chen, Y., and Le, H. (2022), ICON observations of
 547 equatorial ionospheric vertical ExB and field-aligned plasma drifts dur-
 548 ing the 2020-2021 SSW. *Geophysical Research Letters*, 49, e2022GL099238,
 549 doi:10.1029/2022GL099238
- 550 Zulicke, C., Becker, E., Matthias, V., Peters, D.-H.-W., Schmidt, H., Liu, H. L., et
 551 al. (2018), Coolings in observations and simulations coupling of stratospheric
 552 warmings with mesospheric coolings in observations and simulations. *Journal*
 553 *of Climate*, 31(3), 1107-1133, doi:10.1175/jcli-d-17-0047.1

Figure 1.

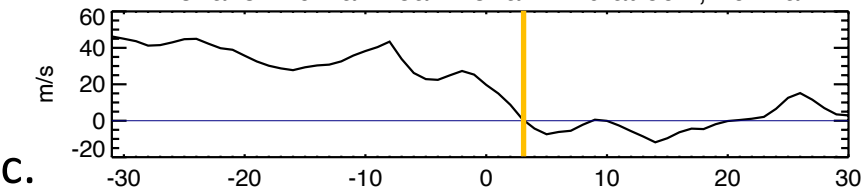
MERRA-2 Zonal & Diurnal Mean U, 60N



MERRA-2 Zonal & Diurnal Mean T, 60N-90N



Zonal & Diurnal Mean Zonal Wind at 60N, 10hPa



F10.7 (black), Kp (blue)

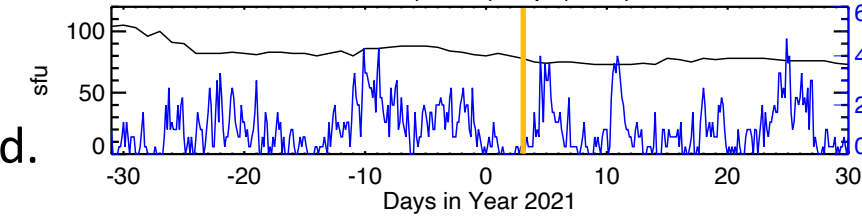


Figure 2.

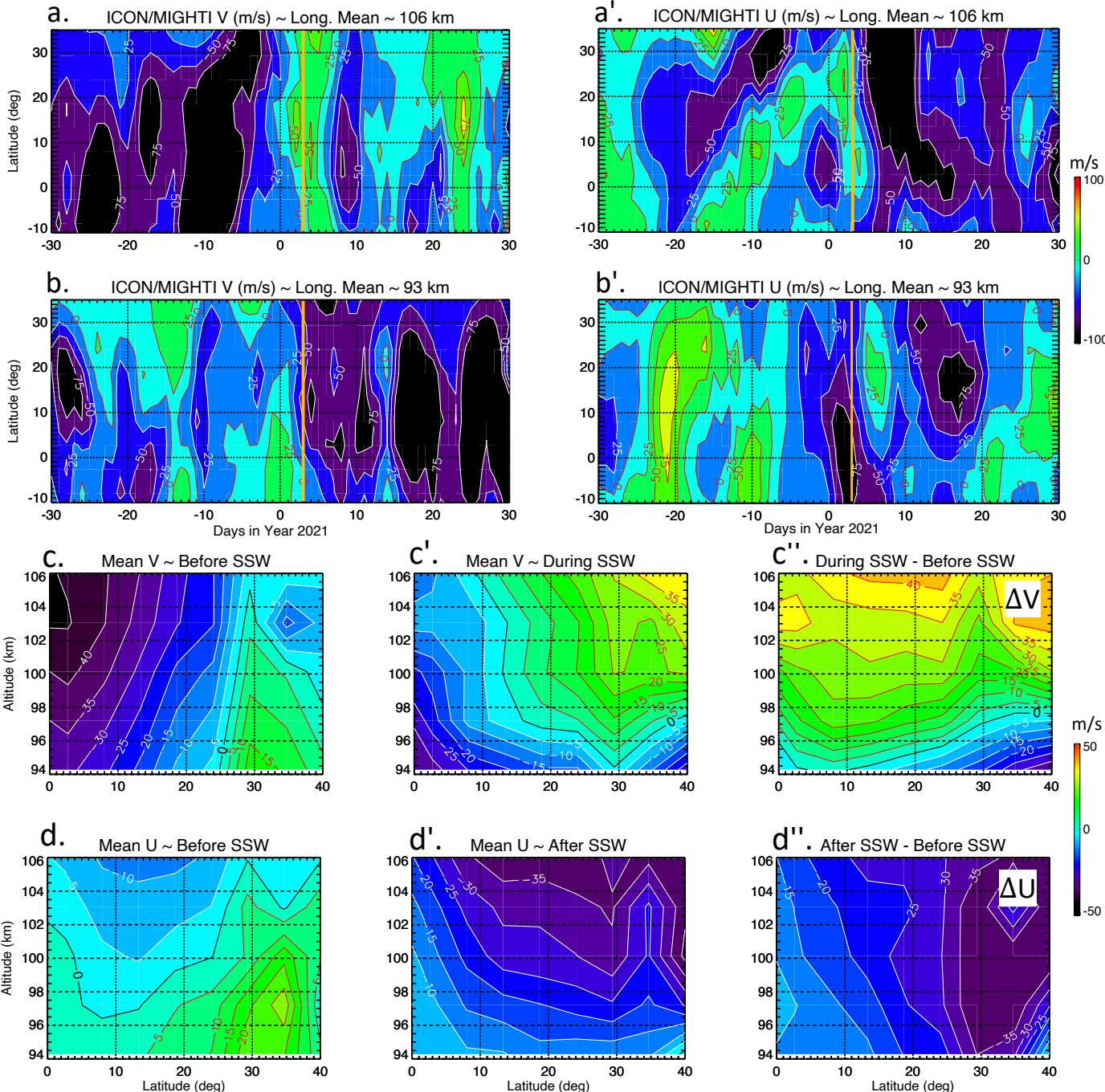


Figure 3.

